A Study of Bypass Transition in a Zero-Pressure Gradient Boundary Layer Subjected to Free stream Turbulence

Vejapong Juttijudata[*1] and Sirod Sirisup[2]

[1] Department of Aerospace Engineering, Faculty of Engineering, Kasetsart University, Bangkok, Thailand 10900

[2] Large Scale Simulation Research Laboratory, National Electronics and Computer Technology Center, National Science and Technology Department Agency, Ministry of Science and Technology, Pathumthani, Thailand 12120

* Corresponding Author: E-mail: vejapong.j@ku.ac.th

Tel: 02 942 8555 Ext. 1708, Fax: 02 579 8570,

Abstract

Bypass transition induced by freestream turbulence has been investigated using the direct numerical simulation (DNS) data of a zero-pressure gradient boundary layer. The DNS data are provided by T. A. Zaki's group, at Imperial College London. The choice of the zero-pressure gradient boundary layer allows the study to focus on the effect of freestream turbulence exclusively. The boundary layer is subjected to 3.5% freestream turbulence at the inlet of the computational domain where Reynolds number based on 99% boundary layer thickness is 800, it undergoes a bypass transition further downstream and eventually becomes fully-turbulent toward the outlet of the domain. A proper orthogonal decomposition analysis of the fluctuating velocity field is carried out in order to objectively extract the most-energetic structures (coherent structures) in the boundary layer and their energy contents. The first five dominant structures carrying 10% of fluctuating energy are composed of important structures such as elongated streamwise streaks or perturbation jets, also known as Klebanoff modes, turbulent spots and traveling-waves. The first five mode description is able to capture almost all the processes in bypass transition except the receptivity of the freestream turbulence into the boundary layer and the formation of Klebanoff modes. Future study in the seek of coherent structures associated with the receptivity and the formation of Klebanoff modes will be undertaken in order to obtain a compact description of bypass transition in a zero-pressure gradient boundary layer.

Keywords*:* bypass transition, freestream turbulence, proper orthogonal decomposition (POD), coherent structures.

1. Introduction

Under an elevated level of freestream turbulence (1% or more), the slow Tollmein-Schlichting wave mechanism may be bypassed leading to a rapid bypass transition process. Since bypass transition has many important applications in engineering, many studies are devoted to study bypass transition (see review article [1]). The process of bypass transition may be divided into three interacting processes: (a)

the receptivity of freestream turbulence into the boundary layer (see review article [2]), (b) the formation and amplification of streaks - streamwise elongated streaky structures of alternating high and low fluctuating streamwise velocity, also known as Klebanoff or breathing modes, (see [3-5]) and (c) the breakdown of streaks (see [6]). Due to the non-linearity process of bypass transition, linear analyzes widely used in stability analysis may not be able to give a complete (and compact) description of the bypass transition process. Alternatively, description may be sorted out.

In the light of coherent structures, complex transitional boundary layers may be decomposed into coherent motion or coherent structures [7] allowing the backbone of transition processes to be extracted out. Many techniques have been used to identify coherent structures in transitional and turbulent flows. The proper orthogonal decomposition (POD) is one of the most successful techniques to objectively extract the most energetic structures defined as coherent structures in the flow [7]. The POD and POD-based reduced-order models shed light on turbulence production mechanisms in many flows (see review in [7]) as well as transition process of natural transition in a zero-pressure gradient boundary layer [8,9] and recently bypass transition in a zero-pressure gradient boundary [10]. Unfortunately, the POD analysis in [10] is obtained from two-dimensional data of PIV in small regions in the boundary layer; a complete picture of bypass transition process from POD view point is still unrevealed. Study [11] performed the POD analysis of transition processes in a complex flow through a compressor cascade using the DNS of [12]. POD could capture Klebanoff modes and traveling wave modes in bypass transition on pressure side and those modes in separation-induced transition on suction side. Nevertheless, such a complex flow needs more modes to fully describe the whole processes of bypass transition on a pressure side and separation-induced transition on a suction side.

The objective of this study is to identify coherent structures in bypass transition process of a zero-pressure gradient boundary layer by means of the POD. The study focuses on the analysis of three-dimensional data covering laminar, transition and turbulent regions in order to obtain a complete description of transition process in a unified framework.

2. DNS of bypass transition in a zero-pressure gradient boundary layer

In this study, the database for the analysis is from DNS of bypass transition in a zero-pressure gradient boundary layer is provided by T. A. Zaki's group, at Imperial College, London. The parameters in the DNS are similar to those reported in [13] and summarized here. Note that *x*, *y* and *z* denote streamwise, vertical and spanwise directions. All the velocity and length in the simulation are normalized by freestream velocity, U_0, and 99% boundary layer thickness at the inlet of the domain, δ_0. The flow domain is a rectangular box in Cartesian coordinate with the dimension of 600 δ_0 x 40 δ_0 x 30 δ_0 in *x*, *y* and *z*, respectively Flow starts from perturbed Blasius velocity with the Reynolds number of 800 at inlet and is convected through the domain. Note that there is no leading edge of the plate in the

simulation (see more detail in [13]). Freestream turbulent intensity is 3.5% at the inlet plane with the integral length scale of 1.8 δ_0. The simulation is based on a central difference formulation on a staggered grid. A fractional step algorithm is employed. Time integration is achieve by a semi-implicit time stepping scheme with third-order Runge-Kutta scheme for explicit terms and Crank-Nicolson scheme for implicit terms. Note that both convective and diffusion terms in a horizontal plane are treated explicitly whereas those in vertical direction are treated implicitly with linearized convective terms to make them partially implicit (see more detail in [13]). The number of grid point is 2051 x 195 x 195 in *x*, *y* and *z*, respectively. Note that the grid in *x* and *z* is uniform. The result is validated against DNS data from [13].

Skin-friction coefficient of the zero-pressure gradient boundary layer is shown in Fig. 1. If the onset of transition is defined as the point of minimum skin-friction coefficient and the completion of transition is defined as the point of its maximum, then the DNS result shows that transition starts at *x* = 220 δ_0 and completes at *x* = 550 δ_0. Velocity perturbation from the mean velocity (x- and y-components) in Fig. 2 shows the presence of elongated streaks or Klebanoff modes starting from the pre-transitional region and continuing all the way through the transition region. Turbulent spots are also observed sporadically in space and time downstream of the streaks. Even though transition starts at 220 δ_0, turbulent spots become mature and can be clearly detected at around *x* = 320 δ_0 . They merge further downstream and become fully turbulent.

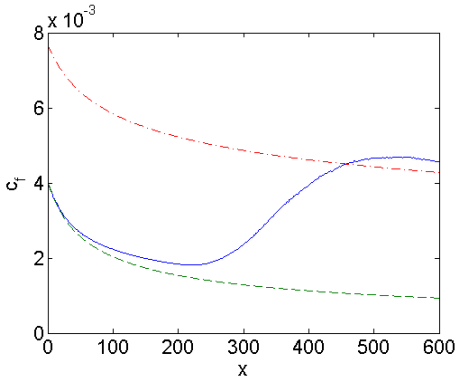

Fig. 1 Skin-friction coefficient: blue-solid line is from DNS result, green-dashed line and red-dashed-dotted line are from empirical correlation.

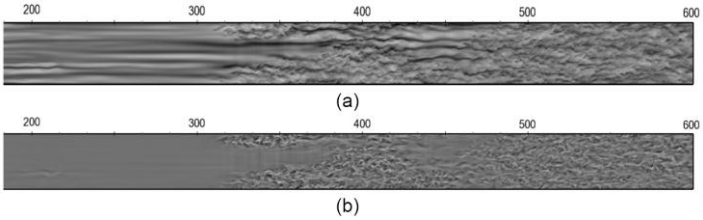

Fig. 2 Contours of streamwise (in (a)) and vertical (in (b)) velocity perturbation on the plane of *y* = δ_0 corresponding to y/δ ~ 0.25 in transition region. The figure shows the region *x* = 200 δ_0 – 600 δ_0 to highlight the transition process starting from *x* = 220 δ_0 - 550 δ_0. Light and dark shades are corresponding to negative and positive values, respectively.

3. Proper orthogonal decomposition (POD)

In order to extract coherent structures from a given ensemble of the given flow fields, the method of "snapshots" [14] is employed. Specifically, let ***V(x,t)*** be a given flow field and the ensemble $\{\boldsymbol{V}(\boldsymbol{x},t_k)\}_{k=1}^{N}$ be a collection of such flow field at observation time t_k for *k=1,...,N* i.e. the flow "snapshots". By decomposing the flow field into mean velocity, $\boldsymbol{U_0}$, and velocity fluctuation, ***u(x,t)*** i.e. ***V(x,t)*** = $\boldsymbol{U_0}$ + ***u(x,t)***, the eigenmode Φ_i may be defined as

$$\Phi_i = \sum_{k=1}^{N} w_k^i u^k, i = 1,\ldots,N \cdot \quad (1)$$

Here, $\boldsymbol{u^k} = \boldsymbol{u(x,t_k)}$ is the velocity fluctuation at time t_k and w_k^i are the components of the eigenvector $\boldsymbol{W}^i$ derived from the eigenvalue problem

$$CW = \lambda W \quad (2)$$

where, $\boldsymbol{C}$ is the spatial correlation matrix defined by

$$C_{ij} = \frac{1}{N}\int_{\Omega} u^i \cdot u^j d\Omega \cdot \quad (3)$$

The eigenvalue corresponding to each eigenvector from Eq. (2) represents the energy content in that eigenvector and eigenmode. Here *u*, *v* and *w* are velocity components in streamwise, vertical and spanwise directions, respectively.

4. Results

The POD is performed on the DNS data at every other grid point from the time span of 8000 δ_0/U_0 (corresponding to 13.3 flow through time, L_x/U_0) constituting 500 snapshots equally separated in time in the ensemble. The data are in a double precision format. The eigenvalue solver used is a double precision LAPACK eigenvalue solver for symmetric matrix. The convergence test and spectral analysis show that, at least, the first five eigenvalues and eigenmodes are converged to their true eigenvalues and eigenmodes; the result and discussion presented focus on those from the first five modes containing 10% of total energy.

The normalized eigenvalues i.e. energy content in each mode relative to the total energy content in the flow are shown in Fig. 3. The most energetic structures (the first and second modes) contain 6% of energy considered to be relatively low compared to those eigenvalues of POD from other non-turbulent flows reported in the literature including a similar bypass transitional flow in [10]. The eigenvalues decay as the order of the eigenmode is increased but nevertheless the decaying rate is not as rapid as those in other non-turbulent flows reported in the literature including those in [10]. The low energy content and slow decaying rate of energy suggest that the flow in this study can be relatively complex. By comparing the energy content in the first few modes, the bypass transitional flow in this study may indeed be as complex as turbulent flows (see the energy content of the first few eigenmodes of turbulent minimal flow unit in [15] for example).

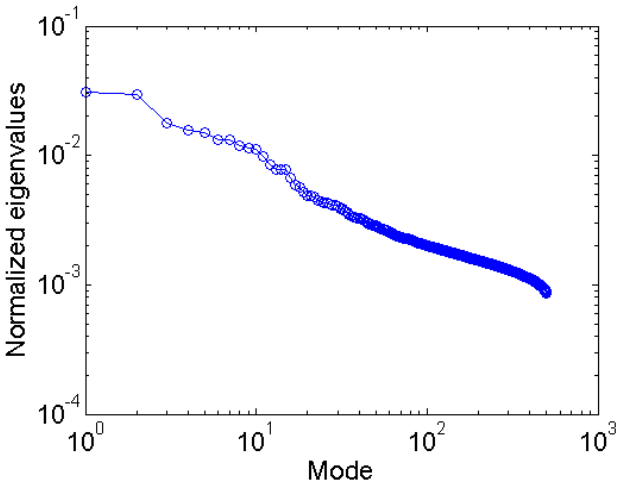

Fig. 3 Energy distribution (normalized eigenvalues) of different POD modes.

Relatively low energy contents in energetic eigenmodes and the slow decaying rate of eigenvalues in this study compared to those in [10] have to be viewed with caution. Despite that the flow in this study and those in [10] are similar, the POD in this study is performed with the whole three dimensional data covering laminar, transition and turbulent regions whereas the POD in [10] is performed with slices

of two-dimensional data covering small regions in pre-transition and low-intermittent regions. Three-dimensionality and diversifying kinematics and dynamics in laminar, transition and turbulent regions enrich the spatial structures and dynamics of the eigenmodes in this study. Clearly, low energy content and the slow decaying rate of the eigenvalues from this study are expected.

The eigenvalues from the first two modes in Fig. 3 are nearly degenerate suggesting that these two modes are pairwise traveling waves. The eigenvalues from mode 3, 4 and 5 are quite close to each other suggesting they contain more-or-less the same amount of energy. Spectral analysis of temporal modes i.e. the eigenvector from Eq. (2) and the visualization of spatial modes i.e. from Eq. (1) are further conducted to gain a better understanding in these eigenmodes.

Fig. 4 shows the energy spectrum of the eigenmodes. It is noted that only the first four energetic frequencies of every eigenmode are shown in the figure. There are nine energetic frequencies associated with these five modes. However, only four of them contain significant amount of the energy in comparison with the rest of the frequencies. namely 0.0006 U_0/δ_0, 0.0019 U_0/δ_0, 0.0021 U_0/δ_0, and 0.0043 U_0/δ_0 corresponding to the time scales of 1600 δ_0/U_0, 530 δ_0/U_0, 470 δ_0/U_0, and 240 δ_0/U_0, respectively. The frequency with the highest energy is 0.0019 U_0/δ_0 associating with every mode except mode 3. Each of the other three frequencies is also associated with at least two modes. Evidently, the dynamics of the modes are rather complicated and suggest active interaction among different eigenmodes.

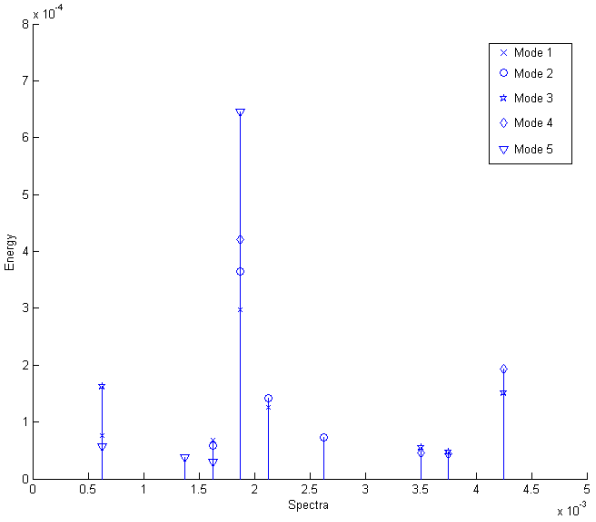

Fig. 4 Energy spectrum of dominant eigenmodes.

Iso-surfaces of the velocity magnitudes of spatial modes are shown in Figs. 5 to 9, consecutively. To further appreciate inter-relation of these spatial modes, contours of the spatial modes on z- and y-planes are shown in Figs. 10 and 11, respectively. It is noted that z-plane is a cut at z = 15 δ_0 through the middle of the domain dividing the domain into equal left and right halves, and y-plane is a cut through y = 1 δ_0 corresponding to y ~ 0.25 δ in transition region. The cut in y-plane underlines relative positions of these eigenmodes in vertical direction as well as streamwise direction whereas the cut in z-plane underlines elongated streaks around y ~ 0.25 δ in transition zone of these modes. The spatial modes of these eigenmodes are quite complicated and cannot be clearly identified as isolated coherent structures reported in the literature.

From the energy spectrum (Fig. 4), mode 1 and mode 2 are dominated by

frequencies of 0.0019 U_0/δ_0 and 0.0021 U_0/δ_0 corresponding to the time scales of 530 δ_0/U_0 and 470 δ_0/U_0, respectively. The spatial modes of mode 1 and 2 (Figs. 5, 6, 10 and 11) are indeed similar but shifted in downstream direction. The matching of two frequencies and spatial modes strongly implies that mode 1 and 2 are traveling wave modes. The structures dominated in mode 1 and 2 consist of streaks and turbulent spots. Both wall streaks and lifted-up streaks locating at the streamwise distance of 350 δ_0 – 450 δ_0, which is in the neighbor where a turbulent spot is mature and merging with the neighbor spot (Fig. 2), are observed. Turbulent spots are detected at the location of 400 δ_0 – 550 δ_0 in streamwise distance. The turbulent spots move at the speed of approximately 0.56 U_0 and spread at the angle of approximately 8° agree well with those reported in the literature (0.6 U_0 and 8°, respectively [16]). However, the precise speed and spreading angle cannot be taken at this point as the boundaries of the turbulent spots are subjected to the level of iso-surface of velocity magnitude defined. Note that from the energy spectrum, the dominant frequencies of mode 4 and 5 are also 0.0019 U_0/δ_0 (Fig. 4). In fact, mode 5 is the most dominated one in this frequency. The spatial mode 5 in Figs. 9, 10 and 11 show that this mode is dominated by streaks in this region as well. Similarly, from Figs. 8, 10 and 11, one of dominated structures in the spatial mode 4 is streaks in this region. Clearly mode 1, 2, 4 and 5 represent the evolution of streaks and their lifting-up at the frequency of 0.0019 U_0/δ_0. In the same time, mode 1 and 2 also represent the evolution of turbulent spot at the frequency of 0.0021 U_0/δ_0.

Mode 4 has another dominated frequency at 0.0043 U_0/δ_0 corresponding to the time scale 240 δ_0/U_0 (Fig. 4). This frequency coincides with one of the dominant frequencies of mode 3. Note that this frequency is close to the frequency of local turbulence in the boundary layer (0.0052 U_0/δ_0) and local freestream turbulence (0.0045 U_0/δ_0.). Thick structures originated slightly above the wall and extended up to almost the edge of the boundary layer present in the spatial modes of mode 3 and 4 in Figs. 7, 8, 10 and 11 (the streaky structure of mode 3 also present but they do not exhibit a traveling wave nature with mode 4; thereby excluding from the thick structures of interest and further discussion below). To be precise, mode 3 contains two thick structures locating at 450 δ_0 – 600 δ_0 in streamwise direction, in the late transition region, and mode 4 contains 450 δ_0 – 500 δ_0, once again in the late transition region. Evidently these two modes are shifted downstream and exhibiting another traveling wave structures. As they reside close to fully turbulent region and are dominated by frequency close to those of either local turbulence or freestream turbulence, the thick structures of mode 3 and 4 should represent the breakdown of streaks into turbulent spots itself at the frequency of 0.0043 U_0/δ_0. Note that the streaky structures in mode 4 have been inferred to be governed by frequency of 0.0019 U_0/δ_0; thereby excluding from these thick structures governed by 0.0043 U_0/δ_0.

The other dominant frequency of mode 3 (Fig. 4) is 0.0006 U_0/δ_0 corresponding to the time scale of 1600 δ_0/U_0 which is relative long and almost three flow through time. By excluding thick structures in mode 3 governed by the frequency of by 0.0043 U_0/δ_0, the left-over spatial structure in mode 3 is streaky structure (Figs. 7, 10 and 11). This streaky structure seems to originated from pre-transition zone around 100 δ_0 and extended up to 300 δ_0 as clearly illustrated by the contour on z-plane shown in Fig. 11. This streaky structure is resembled to Klebanoff modes commonly reported in the literature. By carefully consider the energy spectrum in Fig. 4 and spatial modes in Fig. 11, mode 1 and 5 also have high-energy levels at this frequency of 0.0006 U_0/δ_0 and elongated streaky structures starting in pre-transition to transition regions i.e. Klebanoff mode (mode 1 may not have a strong streaky structure compared with mode 3 and 5, nevertheless). Most likely mode 3, 5 and 1 represent the evolution of Klebanoff modes at the frequency of 0.0006 U_0/δ_0 (but not how they are generated).

Fig. 5 Isosurface of the velocity magnitude at the value of 0.005 of spatial mode 1. The left side of the domain is corresponding to x = 200 δ_0.

Mode 1 – 5 also have high-activity in inlet region as seen in Figs. 10 and 11 (the actual levels of the contour can be not taken literally as the strength of streamwise velocity as the full reconstruction requires amplitudes of all the modes). They may be representing receptivity process of bypass transition but no solid conclusion can be drawn here. It is interesting to see if POD analysis will be able to provide physical insight into the role of low- and high-frequency vortical disturbances in bypass transition as found in [17]. Further analysis has to be carried out.

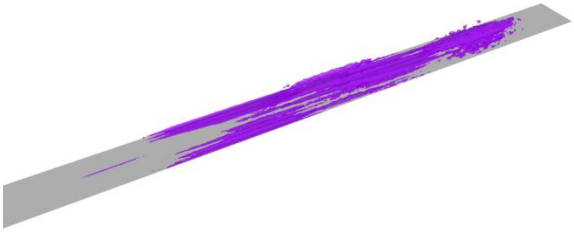

Fig. 6 Isosurface of the velocity magnitude at the value of 0.0050 of spatial mode 2. The left side of the domain is corresponding to x = 200 δ_0.

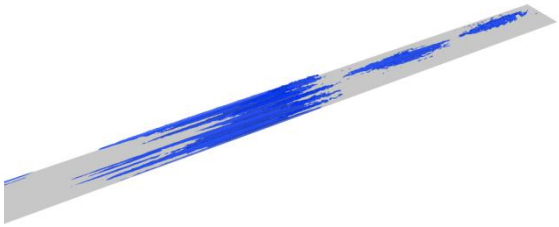

Fig. 7 Isosurface of the velocity magnitude at the value of 0.0065 of spatial mode 3. The left side of the domain is corresponding to x = 200 δ_0.

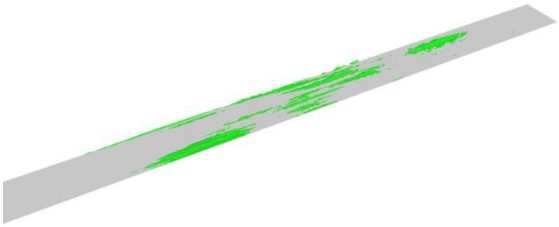

Fig. 8 Isosurface of the velocity magnitude at the value of 0.0065 of spatial mode 4. The left side of the domain is corresponding to x = 200 δ_0.

Fig. 9 Isosurface of the velocity magnitude at the value of 0.0065 of spatial mode 5. The left side of the domain is corresponding to x = 200 δ_0.

5. Conclusion and remarks

The coherent structures of a bypass transition in zero-pressure gradient boundary layer are extracted from DNS data provided by T. A. Zaki's group, at Imperial College London with similar parameter to [13] by means of the POD. The sparse distribution of the eigenvalues indicates that the flow is relatively complex and required many modes to accurately capture its dynamics. Nevertheless the first five modes are able to capture almost all the processes in bypass transition including the evolutions of Klebanoff mode (mode 3, 5 and 1), streaks and their lifting-up close to streak breakdown (mode 1, 2, 4 and 5), streak breakdown (mode 3 and 4), and turbulent spot (mode 1 and 2). Only the receptivity of the freestream turbulence into the boundary layer and the formation of Klebanoff modes are missed out from the first five modes description.

Further analysis on higher-order modes and the reconstruction of the velocity from these coherent structure modes will have to be carried out. In particular, the search of modes representing the receptivity and the formation of Klebanoff modes has to be done in order to arrive at a true compact description of bypass transition in a zero-pressure gradient boundary layer.

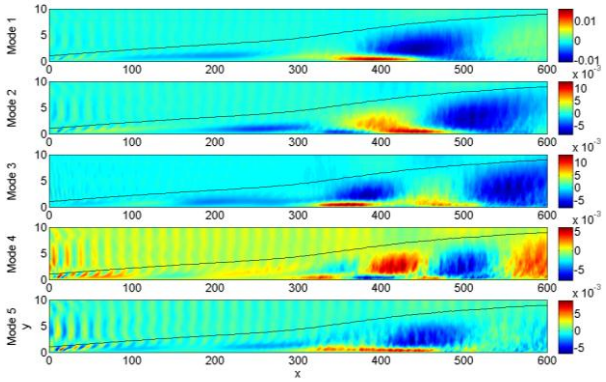

Fig. 10 Contours of streamwise-component of velocity of spatial modes on z-plane at z = 15δ_0 (mid-plane).

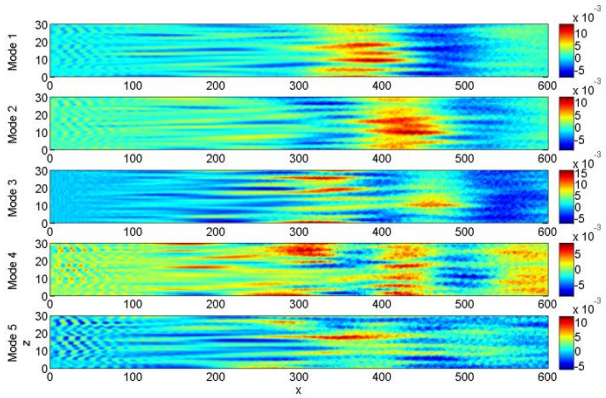

Fig.11 Contours of streamwise-component of velocity of spatial modes on y-plane at y =1 δ_0 corresponding to y/δ ~ 0.25 in transition region.

6. Acknowledgement

Authors would like to acknowledge Dr. Tamer Zaki at Imperial College London for providing the DNS database for this study and providing many assistance and suggestion. VJ would also like to express his gratitude to Dr. Chawalit Kittichaikarn for many discussions on bypass transition and turbulent spots. The authors would also like to express their gratitude to the HPC services from the Large-scale Simulation Research Laboratory of National Electronics and Computer Technology center and WATA Cluster of Faculty of Engineering, Kasetsart University for providing computing resources for this project.

7. References

[1] Durbin, P. and Wu, X. (2007). Transition Beneath Vortical Disturbances, *Ann. Rev. Fluid Mech.*, Vol. 39, pp. 107 – 128.

[2] Saric, W.S., Reed, H.L. and Kerschen, E. (2002). Boundary-Layer Receptivity to Freestream Disturbances, *Ann. Rev. Fluid Mech.*, Vol. 34, pp. 291 – 319.

[3] Andersson, P., Berggren, M. and Henningson, D.S. (1999). Optimal Disturbances and Bypass Transition in Boundary Layers, *Phys. Fluids*, Vol. 11, No. 1, pp. 134 – 150.

[4] Luchini, P. (2000). Reynolds-Number-Independent Instability of the Boundary Layer over a Flat Surface: Optimal Perturbations, *J. Fluid Mech.*, Vol. 404, pp. 289 – 309.

[5] Tumin, A. (2001). A Model of Spatial Algebraic Growth in a Boundary Layer Subjected to a Streamwise Pressure Gradient, *Phys. Fluids*, Vol. 13, No. 5, pp. 1521 – 1523.

[6] Andersson, P., Brandt, L., Bottaro, A. and Henningson, D.S. (2001). On the Breakdown of Boundary Layer Streaks, *J. Fluid Mech.*, Vol. 428, pp. 29 – 60.

[7] Holmes, P., Lumley, J. L. and Berkooz, G. (1996). *Turbulence, Coherent Structures, Dynamical Systems and Symmetry*. Cambridge University Press, Cambridge, UK.

[8] Rempfer, D. and Fasel, H. F. (1994). Evolution of Three-Dimensional Coherent Structures in a Flat-Plate Boundary Layer, *J. Fluid Mech*, Vol. 260, pp. 351 – 375.

[9] Rempfer, D. and Fasel, H. F. (1994). Dynamics of Three-Dimensional Coherent Structures in a Flat-Plate Boundary Layer, *J. Fluid Mech*, Vol. 275, pp. 257 – 283.

[10] Mandal, A.C., Venkatakrishnan, L. and Dey, J. (2010). A Study on Boundary-Layer Transition Induced by Free-Stream Turbulence, *J. Fluid Mech*, Vol. 660, pp. 114 – 146.

[11] Juttijudata, V. and Sirisup, S. (2010). Coherent Structures of Transitional Boundary Layers in a Linear Compressor Cascade, paper presented in *The First TSME International Conference on Mechanical Engineering, 2010*, Ubon Ratchathani, Thailand.

[12] Zaki, T.A., Wissink, J.G., Rodi, W. and Durbin, P.A. (2010). Direct Numerical Simulations of Transition in a Compressor Cascade: The Influence of Free-Stream Turbulence, *J. Fluid Mech.*, Vol. 656, pp. 57 – 98.

[13] Jacobs, R.G. and Durbin, P.A. (2001). Simulations of Bypass Transition, *J. Fluid Mech.*, Vol. 428, pp. 185 – 212.

[14] Sirovich, L. (1987). Turbulence and the Dynamics of Coherent Structures: Part I-III, *Quaterly of Applied Mathematics*, Vol. 45(3), pp. 561 – 590.

[15] Webber, G.A., Handler, R.A. and Sirovich, L. (1997). The Karhunen-Loeve Decomposition of minimal channel flow, *Phys. Fluids*, Vol. 9, pp. 1054 – 1066.

[16] Mayle, R. E. (1991). The Role of Laminar-Turbulent Transition in Gas Turbine Engines, *ASME J. Turbomach*, Vol. 113, October 1991, pp. 509 – 536.

[17] Zaki, T.A. and Durbin, P.A. (2005). Mode Interaction and the Bypass Route to Transition, *J. Fluid Mech*, Vol. 531, pp. 85 – 111.